UNIVERSITY OF BRISTOL

University of Bristol - Explore Bristol Research
General rights

Accepted Manuscript

Title: The effect of sample preparation on uranium hydriding

Author: A. Banos C.A. Stitt T.B. Scott
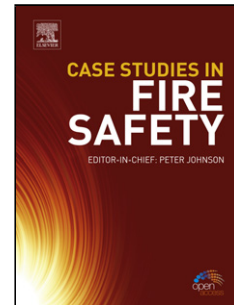
Please cite this article as: A.Banos, C.A.Stitt, T.B.Scott, The effect of sample preparation on uranium hydriding, Corrosion Science http://dx.doi.org/10.1016/j.corsci.2016.10.007

The effect of sample preparation on uranium hydriding

A. Banos [a,] C.A. Stitt [a,] T.B. Scott [a]

[a] University of Bristol, Interface Analysis Centre, School of Physics, HH Wills Physics Laboratory, Tyndall Avenue, Bristol, BS8 1TL, United Kingdom; e-mail: antonis.banos@bristol.ac.uk

[*]Corresponding Author

Additional E-mail of corresponding Author – antonisbanos@gmail.com

Highlights

- Distinct differences in uranium hydride growth rates and characteristics between different uranium surface preparation methods.
- The primary difference between the categories of sample preparations is the level of strain present in the surface.
- The greater the surface-strain in the sample, the higher the nucleation density number, indicating a preferred attack of strained versus unstrained metal.
- As the strain is reduced in the chemically etched samples, surface features such as carbides and grain boundaries were observed to become of much greater importance in controlling nucleation location.

Abstract

The influence of sample cleaning preparation on the early stages of uranium hydriding has been examined, by using four identical samples but concurrently prepared using four different methods. The samples were reacted together in the same corrosion cell to ensure identical exposure conditions. From the analysis, it was found that the hydride nucleation rate was proportional to the level of strain exhibiting higher number density for the more strained surfaces. Additionally, microstructure of the metal plays a secondary role regarding initial hydrogen attack on the highly strained surfaces yet starts to dominate the system while moving to more pristine samples.

Introduction

Radioactive intermediate level wastes arising from the UK civil nuclear programme, including reactive metals such as uranium metal and Magnox cladding have continually been accumulating for up to 60 years. Due to the constantly increasing amount of this material, there is an urgency to underpin the safety of the oldest wastes by better understanding their physicochemical state. This knowledge also supports future retrieval and repackaging of selected wastes, better preparing them for long-term storage and disposal. Uranium hydride (UH_3) formation is a potential yet unwanted corrosion occurrence indirectly resulting from wet oxidation [1]. The highly unstable nature of UH_3 when exposed to air [2] raises serious environmental and technical challenges with respect to the safe handling and treatment of these by-products should they have formed.

From the literature [3], it is well known that the uranium-hydrogen reaction can be divided into four distinct stages:

1

i. An induction period where initial hydrogen adsorption occurs. This period extends from the time of hydrogen exposure to when the first nuclei appear on the metal surface.
ii. A nucleation and growth period where discrete UH_3 sites begin to form and grow (Accelerating stage).
iii. A bulk reaction where coalescence of the hydride sites results in a homogeneous reaction front moving into the surface (Linear stage).
iv. A termination period where complete transformation of the metal to UH_3 is observed (Decelerating stage).

It has been observed that the initial transformation of uranium to UH_3 occurs in a spot-wise manner and usually at preferred locations on the metal surface which encourage physi-sorption, dissociation and diffusion of hydrogen gas (H_2) [4]. These are referred to as low energy diffusion and trapping sites.

There have been many studies concentrated on deriving the uranium-hydrogen reaction rates under various environmental conditions, therefore the linear stage of the reaction has been thoroughly studies [5-14]. However, the initial reaction phase, where rates are accelerating rapidly is far more complex due to the many factors effecting hydride spot initiation and growth [4, 15-23]. It has thus proven much more challenging to examine. According to the literature, common parameters such as the induction period, the nucleation rate, the hydride growth and the location of the hydrides are influenced by a number of factors [4, 15-23]. To initiate the uranium-hydrogen reaction, hydrogen has to diffuse through a naturally occurring oxide layer covering the metal surface and nucleate at the metal-oxide interface [24]. The induction period is extended with increasing oxide thickness [19]. Additionally, the purity and stoichiometry of the growing oxide controls the initiation time and the nucleation density of the hydrides [19]. This is because impurities are considered to block potential sorption sites and diffusion pathways to the metal [19]. The purity of the reactant gas was also found to prolong the induction period owing to the competition of impurity entities (O_2, H_2O, N_2, CO_2 etc.) with H_2 on the available sorption sites [16]. Another important factor, which effects the early hydriding stage, is the reactant gas pressure and temperature [3]. Elevated pressures and temperatures were found to shorten the induction time [3]. However, the temperature effect is far more pronounced providing that the experiment temperature is close to where maximum hydriding rates are observed (T=160-250 °C) and hydrogen is abundant in the system [15]. The nucleation density, which is defined as the number of growing nuclei per mm^2, is finite for every sample and depends on the solubility of hydrogen in uranium and the metal microstructure [15]. Since the diffusivity of hydrogen is enhanced with increased temperature, it is expected that higher temperatures will increase the nucleation rate providing there is a constant H_2 supply [15]. Indeed, experiments by Scott et al. [20] demonstrated very significant nucleation rates at the highest temperature range for hydriding, forming chains of hydride rather than individual spots.

The metal microstructure plays a key role on the nucleation number density and location of hydride growth [18, 20]. Dislocations such as crystallographic slipping planes and twins formed through the fabrication process, along with grain boundaries, provide low energy locations for hydride nucleation and growth [18]. It has been documented that the microstructure of the metal surface is sometimes reflected in the growing oxide; therefore strained or disrupted regions in the metal will appear as discontinued areas on the oxide surface due to the unevenness of the growing oxide [18, 25]. In addition, different oxidation rates have been recorded between metal grains with different crystal direction [25]. The heterogeneity of the oxide thickness leads to induced stress in-between the oxide boundary interface [18]. A similar effect has also been observed at the perimeter of inclusion sites, with an additional source of strain for these areas coming from the different thermal expansion (considerably higher melting point of carbide phases) between the inclusion (UC, UCN and UC_2) and the metal [26]. Thus, it is expected that grain and twin boundaries along with inclusions and other strained regions will be reflected as areas of oxide disruption. Discontinuities in the oxide facilitate hydrogen ingress to the metal, thus promoting on-site nucleation [18]. The above considerations lead to the assumption that a pristine and strain-free surface with large crystallographic grains will provide fewer points of initial hydrogen attack when compared to a strained surface exhibiting small grains, providing both have similar average oxide thickness. Indeed, grain and twin boundaries [15, 20, 24, 27-29] have been identified as early nucleation and growth sites by some investigators and inclusions were also reported as initiation locations by others [4, 18, 28, 30, 31].

It is believed that the interplay of the above factors control the very early hydriding behaviour of uranium metal. Previous studies in the literature have provided indications that strain in the metal or oxide may encourage early initiation of hydride growth [32] but none has yet provided substantial and definitive proof [4, 18]. Following this hypothesis, it was decided to examine the influence of sample cleaning preparation, thus the effect of the surface conditions at the surface, on uranium hydriding at the early stage. Sample preparations involving mechanical abrasion

2

will cause a work-hardened layer to form in the outermost region of the metal surface [24]. The thickness of this layer will depend on the level of the grinding medium used and the mechanical force applied during abrasion [24]. As an alternative, chemically driven processes, which involve metal removal by means of acid dissolution or electrochemically driven anodic dissolution, may produce near pristine surfaces [22, 28]. Nevertheless, surface features such as inclusion particles are significantly disturbed [22] and the composition of the growing oxide may be altered [28]. Little attention has been given by investigators on this matter, despite the numerous different sample preparation techniques been employed by various groups prior to the hydriding reaction [4, 17, 19, 20, 22, 28, 30, 33]. Table 1 summarises the experimental conditions previously used in the available published literature for the uranium-hydrogen reaction. To compare between studies, information such as sample origin, hydriding conditions and cleaning preparation in addition to post-reaction surface examination are included in the table. It is evident that despite similar experimental conditions (temperature and pressure) [17, 20, 22, 24, 30, 33], the growth behaviour of UH_3 differs between research groups, which may be attributable in part, to the sample preparation procedure. Of course, subtle dissimilarities in the metal microstructure [4, 22, 28, 30] or the grown oxide [4, 19, 28] may also be responsible for these discrepancies. In an effort to isolate and focus on the effect of cleaning preparation on uranium hydriding behaviour, four identical samples originating from the same metal coupon were concurrently prepared using four different methods. These samples were reacted together simultaneously such that the temperature, hydrogen exposure time and pressure were identical for each sample, therefore the only variables effecting the hydriding reaction was the condition of the metal surface i.e. level of strain and oxide thickness.

Experimental

Sample characterisation

Unirradiated natural uranium prepared for Magnox fuel was used for the study. The traditional casting method for Magnox-uranium production was to β-quench the cast uranium rods by heating to 660-700 °C and rapidly cooling to room temperature. Electron back-scattered diffraction (EBSD) analysis on the uranium showed a randomly oriented microstructure with multiple grains exhibiting a linear variation in size (figure 1). Grain texture indicates plastic deformation as a result of stresses developed during the fabrication process. The anisotropic thermal properties of uranium combined with the manufacturing process will have caused considerable internal stresses, this is demonstrated by the existence of multiple slip planes, and twin boundaries throughout the crystallographic structure (figure 2a). The samples exhibited a high carbon content with an average of 1045 inclusions per mm^2 on the polished surfaces (figure 2b). Inclusions, usually carbides, of various shapes (X-shaped, H-shaped, cuboid) and sizes (2.5-17 μm in dia.) were spread homogeneously on the surface. Four samples of the same weight and surface area (0.45 g, ~0.8 cm^2) were cut from the same uranium penny using a Struers Accutom cutting machine. This process was expected to induce some localised surficial strain at the cut surface from mechanical disruption caused by the cutting blade.

Surface preparation

After cutting, the four square-shaped samples were mechanically abraded on all sides to a 2-3 μm surface finish (P4000) using silicon carbide papers and water as a lubricant. The samples were then cleaned with water to remove excess debris and four different cleaning preparation methods were employed:

Coarsely finished sample. This sample was stored in an inert atmosphere (Ar-filled glovebox) whilst the other three preparations were employed. When the others were near completion a final re-abrasion to a 2-3 μm finish was achieved.

Finely polished sample. This sample received a fine polish to a ¼-μm finish using diamond paste and oil as a lubricant.

Nitric acid etched sample. This sample was pickled in HNO_3 (5 M) solution for 3 h.

Electropolished sample. The sample was electrochemically etched using a solution containing a 10:6:6 (volume ratio) mixture of ethylene glycol, orthophosphoric acid and absolute ethanol with an applied voltage of 9-10 V and a flowing current of ~0.1 A for 1 min.

It is important to note that a very accurate timetable was implemented in order to complete the preparations for all four samples simultaneously. Subsequently, all samples were washed together in ethanol and ultra-high purity methanol to remove residual surface impurities and then finally weighed. The samples were then all left exposed to air for 45 minutes to ensure that all samples had reached the linear stage of oxide development. This was required to reduce the influence of oxide thickness on the formation of uranium hydride between samples.

Hydriding reaction

After air exposure, all four samples were loaded together in a stainless steel reaction cell and evacuated to $<5 \times 10^{-7}$ mbar. Thin foil sheets were used to encase the samples separately in the cell ensuring no interaction or exchange between the samples took place. Additionally, at the temperatures and pressures of gas used, the proximity of each sample to the gas inlet was not expected to effect the sample hydriding rate. The temperature was raised to 220 °C and left to stabilise for 2 h. This period was considered sufficient for the majority of oxide impurities to desorb but without significant oxide diffusion/ transformation [21, 23] or metal grain growth [17, 33] occurring. A fixed volume of 500 mbar deuterium (D_2) was then introduced to the sample cell. A slight (<1 mbar) decrease in pressure was observed seconds after D_2 introduction and was ascribed to gas absorption to the surface oxide. After approximately 5 min, a 4.32 mbar (equivalent to 0.0076 mmol of D_2) drop in gas pressure was observed, signifying the onset of hydride nucleation and growth. The reaction was immediately ceased, by pumping the reacting gas off the system. That pressure difference was considered as ideal for all four surfaces to exhibit hydride formation ensuring, however, that the reaction will be ceased prior to the bulk reaction stage.

Analysis techniques

Secondary ion mass spectrometry (SIMS)

The ion mass spectrometry work was carried out using a custom-made SIMS instrument. The equipment consisted of a FEI focused gallium ion source fitted to a Vacuum Generators model 7035 double-focusing magnetic sector mass analyser. The analysis was performed in positive ion mode with a 3 nA beam current. The thickness of the oxide was calculated using depth profiling of the U^+, UO^+ and UO_2^+ ion and ion clusters, while UH_3 identification was analysed by obtaining multi-mass ion maps for UH^+ and UD^+ on selected areas on each sample.

Focused ion beam (FIB) milling and rastering

A FEI FIB-201 focused gallium ion source instrument was used for post-hydriding examination of the surface. Cross-sections of the surface, with particular attention to surface features such as inclusions and hydrides, were performed using ion beam milling with high probe currents. Secondary electron (SE) images of the surface and cross-sections were attained using a 30 kV accelerating voltage and a probe current of 70 pA. Ion beam raster scanning was conducted at a 5-10 degrees angle of incidence using a probe current of 6600 pA and a 30 kV accelerating voltage over an area of ~73750 μm^2. Approximately 100 nm of oxide was removed thereby revealing the underlying metal microstructure. This procedure was conducted prior to, and following, surface hydriding of the electropolished sample. This process may have also reduced any residual strain or unevenness of the metal surface.

EBSD analysis – SE images

Samples cut from the original penny were electropolished and analysed in a Zeiss EVO-MA10 scanning electron microscopy (SEM) instrument with a LaB_6 source operating with an accelerating voltage of 30 kV and a probe current of 0.7 nA. EBSD diffraction patterns were acquired on a phosphor control screen using a Digiview 3 high-speed camera and an EDAX- EBSD instrumentation fitted with the orientation imaging microscopy Analysis 6.2 software

for data collection and processing. This allowed us to obtain crystal orientation maps for the non-reacted and partially hydrided surface of the sample.

Results

Samples were investigated for the physicochemical changes occurring on their surface after the hydriding process. Therefore, rigorous analysis was performed prior to, and following, hydrogen corrosion on each of the four samples.

Pre-hydriding analysis

Sample surface after preparation

The samples exhibited distinct differences in their surface finish as a result of the different cleaning preparation methods. On the first sample after mechanical abrasion, the surface was left roughened, with a micro-network of intersecting striation lines. FIB sections (not shown) demonstrated significant work-hardening in the near surface region to a ~3 μm depth. On the finely polished sample, the surface roughness was significantly reduced and was almost free of striation lines. The work-hardened layer was not easily resolved in FIB sections. On the chemically etched samples, work-hardening was absent and the surface pristinely smooth. However, acid etching was observed to significantly reduce the number of surface exposed carbide inclusions (via dissolution), leaving the surface with vacant carbide pits. As will be discussed later in the paper, these vacant pits served as excellent locations for hydride nucleation and growth. Electropolishing resulted in the most pristine surface out of all four samples, however it was previously documented that during this process the oxide covering the metal surface penetrates down the interface of embedded carbide particles [22], resulting in inactivation of carbide peripheries as preferential locations for UH_3 initiation. The scope of this work was to evaluate the early hydriding behaviour of samples prepared with one of the above preparation methods and not to thoroughly study the effects of these methods to the surface. Hence, further investigation of the surfaces at the pre-hydriding stage was not undertaken.

Oxide thickness and composition identification - Depth profiling

It has been reported in the literature that depending on the uranium surface preparation technique, different oxidation rates are achieved, this results in dissimilar oxide thicknesses and varied composition of the growing oxide [4]. If between samples there was a large mismatch in one of these latter parameters, for example the oxide thickness varied over 10 s of nm for comparisons between the 0-50 nm range, then the hydriding behaviour was expected to significantly differ, thus preventing a fair comparison between samples. To better understand the oxidation behaviour on the samples here, the preparation process described in the previous section was repeated and the thickness of the oxide layer was measured after 1 h in air for all four surfaces (table 2). From the analysis, it was found that the nitric acid etched surface oxidised at a faster rate compared to the other samples. This sample exhibited an oxide layer of ~45 nm, whilst the oxide on the electropolished sample was only ~20 nm after 1 h in air. Between air exposure and the hydride reaction, the samples were heated at 220 °C for a 2-hour period in high vacuum and thus the thickness was expected to increase at a slower rate on all four surfaces. With such a great difference in oxide thickness and by assuming that the oxide plays a dominant role in the nucleation rate, we would expect a large scatter in the nucleation rate and number density of the hydrides between the chemically etched samples. However, as explained in the next section, this prediction was not observed in the results, which leads to the hypothesis that other parameters play an important role at this reaction stage.

Post-hydriding analysis

SIMS examination – UH_3 identification

Hydride sites were observed to form on the samples regardless of the employed preparation technique. In each case, positive-ion mode surface scans confirmed the presence of UH^+ and UD^+ ion cluster signals at these locations. Figures

3a-e show an SE image of the surface and the accompanying mass ion maps for the finely polished sample. Blister-like spots are evident emerging from the surface, which are attributed to UH_3 formation and expansion. As expected the UH^+ and UD^+ ion cluster signals coincide displaying ostensibly identical maps while the uranium dioxide (UO_2) signal was weak due to sputtering of the oxide surface. The nucleation number density for each sample was calculated by combining direct measurements of the identified UH_3 sites from SEM, FIB images and SIMS mass ion maps. By examining a very large number of regions, a representative number density was extrapolated for mm^2 area.

SEM – FIB examination

General inspection of the hydriding behaviour observed on each prepared surface determined that the samples could be broadly split into two categories: mechanically finished samples and chemically etched samples. Figures 4a-d illustrate an SE image for all four surfaces in the post-reacted phase. The main distinction between the two categories was the arising hydride morphology and how the hydrides had initiated and grown. The hydriding behaviour of each sample shall now be discussed separately.

Mechanically finished samples

Coarsely finished sample

The coarsely finished sample exhibited the highest nucleation density number per mm^2 of all four surfaces, measuring an average of ~4762 hydrides/ mm^2 (table 3). Only one family of hydrides was identified, which exhibited lenticular and crescent-shape blisters, with a mean diameter of ~21.65 μm. Figure 5a depicts the post-reaction surface of the coarsely finished sample. In some areas, the surface was so densely populated with hydrides that a near-continuous layer had formed (figure 5b). The vast majority of the hydride sites had failed to breach the surface oxide layer (>95 %). Only a small number of somewhat larger hydrides were observed to break the surface oxide layer and each coincided with carbide inclusion particles exposed on the metal surface (figure 5c). Scratches originating from mechanical abrasion during preparation were often intersected by hydride growths (figure 5d) since surface deformation lowered the activation energy of nucleation. FIB sectioning was utilised to identify the hydride nucleation location and depth by direct observation of the hydride cross-section. Investigation of the larger, oxide-breached sites revealed that initial attack occurred at or on the margins of carbide inclusions (figure 6a-c). In summary, the hydrides appeared non oxide-breached, numerous, moderate in size and homogeneously distributed on the coarsely finished uranium surface.

Finely polished sample

Figure 7a shows the finely polished surface after the hydriding process. Despite the large scatter in size (9-42 μm) between the UH_3 sites, only one family of lenticular and crescent-shaped hydrides was observed on the surface. In comparison to the coarsely finished sample, the finely polished sample was dominated by crescent shaped hydrides. The average number density of the hydrides was also significantly lower in comparison to the coarsely finished sample, yet the mean diameter of the spots was higher. Around 20 % of the hydrides had breached the oxide surface, with the majority coinciding with inclusion particles (figure 7b). Indeed, FIB sectioning of numerous hydrides confirmed that almost all burst sites had initiated at carbide inclusions particle sites (figure 8a & b). The non-burst hydrides exhibited a high horizontal growth velocity in comparison to vertical and typically formed at crystallographic grain and twin boundaries (figure 8c & d).

In addition to lenticular shaped hydride blisters, the mechanically finished surfaces also exhibited crescent-shaped hydrides, which were more pronounced on the finely polished sample (figure 9a). Crescent shaped formation was observed for the first time and the driving force of this effect is unknown. FIB cutting and viewing did not reveal any physical features specifically affecting this growth, excluding crystallographic grain and twin boundary sites, which were also found elsewhere (figure 9b & c). It is speculated that some crystallographic orientations of the uranium were easier to form hydrides than others or alternatively, it may be a surface strain-driven effect. Since this type of hydride was more abundant on the finely polished sample, one possible explanation may relate the level of strain and the

6

nucleation density to the final hydride development. If it was assumed that a more strained surface would provide a larger number of low energy or disrupted regions for hydrogen sorption and diffusion, then the higher nucleation density number of the coarsely finished sample with regards to the finely polished sample is justified. Regarding the finely polished sample, the considerably smaller number of nucleation spots for the same area, provide more than enough space for the hydrides to expand and fully develop without being contained from neighbouring hydrides. Of course, for this to happen, the hydrides should not be inhibited by microstructural features like grain and twin boundaries that could potentially generate a barrier on their interface. Another important observation is the very high lateral growth velocity parallel to the surface letting the hydride to develop significantly before bursting the oxide surface. As for the growth mechanism for the crescent shaped hydrides, it seems that after initial formation the sites are not developing concentrically in a uniform manner but instead exhibit slow growth in one direction compared to others. We tentatively ascribe this to preferential hydride propagation in uranium crystal directions (figure 9b).

Chemically etched samples

Nitric acid etched sample

Notably fewer hydride sites were present per mm^2 for the nitric acid etched surface in comparison to the mechanically finished surfaces (table 3). Based on their morphology and size, the hydrides could be split into two groups: a smaller, slower nucleating group (~11.24 μm in average dia.) and a larger, faster nucleating group (~25.8 μm in average dia.) (figure 10a). This behaviour had been previously reported by Bloch et al. [15]. The smaller hydride group comprised hydrides with a complete overlying oxide layer and were located at crystallographic sites exposed in the metal e.g. grain boundaries or crystal twins (figure 10b). The larger diameter sites grew predominantly around carbide particles and were fully or partially erupted through the surface oxide. This behaviour was ascribed to the very high vertical growth rate of the hydrides around the perimeter of inclusion particles, promoting the hydride front to achieve considerable depth into the bulk of the metal. Even though a significant number of inclusions had been consumed during the acid-etching process, the vacant carbide pits were also observed as excellent nucleation and growth locations for hydrides (figure 10c).

Electropolished sample

The electropolished sample showed the greatest corrosion resistance to D_2 in comparison to all the other samples. However, it did exhibit the highest damage per hydride growth, i.e. the surface damage or corrosion progression caused by D_2 from a single hydride was greatest in comparison to the large diameter sites found on the previous three samples (figure 11a). Similar to the nitric acid etched sample, two families of hydrides were observed: a smaller, slower nucleating group (~18.19 μm in average dia.) and a larger, faster growing group (~44.24 μm in average dia.). The large diameter group was comprised of oxide-burst spots coalescing to form hydride growth clusters (figure 11b). The surface exhibited very significant distortion around these growths and it was very difficult to identify the initial nucleation locations. Carbide inclusions were found to accommodate only moderate size hydrides, which partially erupted through the oxide surface (figure 11c).

The surface microstructure of the electropolished sample was revealed by ion sputtering the oxide layer, which permitting identification of the locations for hydride initiation. This technique is only possible on the chemically etched surfaces where the grains and the microstructural features of the sample are left intact below the oxide layer. Figure 12 displays the surface of the partially hydrided and electropolished sample: (a) before and (b) after ion sputtering. It is clear that the majority of the slow nucleating group of hydrides tended to form along crystallographic grain boundaries or dislocations such as twins. EBSD maps of the post-reacted electropolished sample surface similarly confirmed this behaviour (figure 13).

Overall comparison

Between the two sample preparation categories, chemically etched and mechanically finished, there were distinct differences. Fewer hydrides were present per mm^2 on the chemically etched surfaces when compared to the mechanically finished, with the electropolished surface exhibiting the fewest and the coarsely finished sample exhibiting greatest number density (table 2). The mechanically prepared samples displayed only one family of hydrides, while the chemically etched ones exhibited two. The mechanically finished samples exhibited hydrides, which appeared to retain higher horizontal growth velocities (i.e. parallel with the metal surface) in comparison to the

7

chemically etched samples. The vertical growth velocity was moderate by comparison and allowed the hydrides to grow to a considerable lateral dimensions (>25 μm) without bursting through the oxide layer. This phenomenon was more pronounced on the finely polished sample, which exhibited very large yet intact crescent shaped hydrides. In comparison, the chemically prepared samples showed similar growth velocities in all directions, leading to formation of oxide-breached hydrides that subsequently propagated deep into the bulk of the metal (figure 10c & 11b). It is expected that, if the reaction was ceased at a later stage, a fully developed reaction front would form on the surface of the mechanically finished samples, whereas on the chemically etched surfaces a 'pitting type attack' would instead appear [15]. According to Teter et al. [19] the hydride density is expected to be lower and the pitting to be more pronounced on a surface with a thicker oxide layer [19]. By comparing the chemically etched surfaces, we would expect the electropolished surface with a considerably thinner oxide (table 2) to exhibit a higher nucleation density than the nitric acid etched surface however this is not the case here. The electropolished sample has a lower hydride number density and accommodated well-developed hydrides when compared to the nitric acid etched surface. It is possible that the composition of uranium dioxide has varied and this could possibly have effected hydrogen diffusion. However if that is the case, the surface preparation caused the difference and thus plays a key role at this stage and not the variance in oxide thickness.

In an effort to quantify and compare the hydride development characteristics between the four sample preparation scenarios, a new parameter was introduced to the calculations: the lateral to vertical growth velocity or growth shape aspect ratio. This ratio is the hydride growth extent on the axis parallel to the surface (numerator in μm) versus the growth extent in the vertical direction (denominator in μm) (figure 14). The ratio assumes that growth is concentric from a central initiation point at the oxide metal interface [24]. Table 4 illustrates the derived values of ratios for the various types of hydrides. Regarding the values exhibited in this table two things must be considered: (1) the large and small diameter families for the chemically etched samples were distinguished and (2), the aspect ratio for the large diameter family of the electropolished sample had not been derived as single hydride spots could not be easily distinguished (clusters of hydrides).

From the analysis, it was found that the finely polished sample exhibited the highest hydride aspect ratios, in comparison to the hydrides grown on differently prepared samples. Hydrides around inclusion sites exhibited relatively lower aspect ratios as the hydride tended to intrude down the margins of the carbide particles, reaching a considerable depth more easily. The ratio derived from the large family of the nitric acid etched sample displayed the lowest value indicating that oxide breaching due to hydride development was occurring relatively easier on that surface. Comparable ratios were obtained for the small diameter families of the chemically etched samples indicating similar hydriding rates and behaviour for the slow nucleating group of both preparation methods.

Discussion

The results collected here suggest that the early stage corrosion behaviour of the uranium-hydrogen reaction is greatly influenced by the physical state of the metal surface prior to hydrogen exposure. This statement was supported by examining four identical samples that had undergone different surface preparation methods and were then reacted in the same cell under the same reaction conditions. The post-reaction examination showed distinct differences in the early hydriding behaviour between the mechanically finished and chemically etched samples despite the surface oxide thicknesses being comparable. The preparations that involved mechanical abrasion or polishing at the final step of the process always left the surface with a work-hardened layer of a certain thickness [24]. The thickness of this layer depended on the grade level of the polishing medium. Even for very fine polishing, where the work-hardened layer has limited vertical extent, strain in the form of thin and shallow scratching lines and slip twins is apparent to some extent. These points of surface disruption will be reflected in the oxide, subsequently developed on top. Conversely, preparations involving chemical etching using acidic solutions and/ or current flow resulted in a pristine and strain-free surface. Work-hardening and scratches are removed with this method, however in contrast to the mechanically finished samples metal etching, isolates or extracts inclusion particles from the metal matrix.

On the coarsely finished sample surface mechanical disruption, as a result of the cleaning preparation, was far more pronounced than any other surface and resulted in an almost fully hydride-covered surface after hydriding. The disrupted layer developed during the polishing process, provided wide discontinuous areas on the metal where D_2 could easily diffuse in and reach the metal. This resulted in a high nucleation density number and a homogeneous spread of the hydrides on the surface. It is evident that burst hydrides coincided with carbide inclusion locations yet no microstructure effect on the initiation location has taken place on this surface as the hydrides have almost

simultaneously nucleated on the surface disrupted regions. The mean hydride depth was estimated ~3.77 μm (table 4). The finely polished sample surface was less disrupted than the coarsely finished sample and since fewer oxide disruptions were present, hydride nucleation locations were limited, thus, the density number was greatly reduced and the size of the hydrides increased. Two observations are highlighted here: 1) Discreet hydride initiation implies that the metal microstructure may have a greater influence on the surface and 2) High lateral to vertical growth velocity aspect ratio, which in turn suggests that the hydrides did not propagate deep into the surface. It could be speculated that D_2 may diffuse more easily through the work-hardened layer than the bulk metal microstructure, leading to preferential lateral propagation of the hydrides on the finely polished sample. If that statement is true then it may be argued that on the coarsely finished sample where the work-hardened layer is thicker the growth aspect ratio should be large due to enhanced lateral growth velocity. However, this is not the case here. The moderate aspect ratio is a result of (a) uniform hydride growth in all directions both laterally and vertically inside the work-hardened layer and (b) enhanced nucleation rate of the coarsely finished surface due to higher surface strain leading to lateral growth suppression from the neighbouring hydrides with each other (figure 6b & c). Hence, for the mechanically prepared samples, it is believed that it is the level of surface-strain and the thickness of the work-hardened layer that control the early hydriding behaviour.

The chemically etched samples did not display features associated with a work-hardened layer prior to hydriding. Therefore, the above considerations cannot be applied. The nitric acid etched sample exhibited a very smooth surface with a substantial number of carbides particles partially or completely dissolved from the surface. Inclusion particle sites and vacant inclusion sites served as excellent nucleation and growth locations. Around these areas, it was expected that the oxide exhibited discontinuities, producing an uneven thickness at the margins of the inclusions or the vacant locations. On a chemically etched pristine surface, the hydride nucleation density was further diminished in comparison to the mechanically finished samples, and features like carbides, inclusion vacant areas and grain and twin boundaries dominated the hydride initiation locations. Since the nucleation number density was lower, and the hydrides exhibited on the surface were much larger than observed elsewhere, the amount of D_2 gas consumption per hydride was greater. This was sufficient to produce hydride volumes that caused enough strain in the overlying oxide to fracture it, even for the smaller nucleating family. It is speculated that the absence of the work-hardened layer reduced UD_3 nucleation due to fewer disruptions in the overlying oxide. This may have also been the reason for a greater destruction at the hydride nucleation site yet more on-site detrimental for the metal if nucleation occurred. The electropolished sample exhibited the fewest hydride sites per area; however, the oxide disruption surrounding each hydride site was the greatest out of all four surfaces. With regards to the large nucleating family, attack around carbide particles was evident, however consistent with previous studies not all the inclusions were attacked [22]. EBSD measurements indicated that the surface was highly crystallographically textured, exhibited multiple twins and displayed high carbon content, therefore, it is possible that the initiation location attributed to a carbide also coincided with a crystal twin or a grain boundary. Grain boundaries and twins were determined as the dominant influence for aiding the growth of the small diameter nucleating group with the majority of the sites observed to form around these areas (figure 12-13). Since the uranium exhibited a high carbon content, it was probable that the hydrides formed close if not around inclusion sites. In any scenario, if the grown hydride reaches the margins of the carbide a change in the mechanism of hydrogen diffusion is likely to happen as carbide inclusions are assumed to provide preferential pathways for hydrogen diffusion into the metal compared to a flat surface [28, 30]. These areas are thought to act as hydrogen 'sinks', encouraging rapid hydrogen diffusion through existing hydrides rather than into new nucleation centres. This preference of further hydride growth through existing sites has recently been proven by Jones et al. [34] working on depleted uranium. As a result, the erupted sites of the chemically etched samples displayed a greater vertical growth velocity, perpendicular to the metal surface over the lateral velocity. This behaviour is opposite to that observed for the mechanically finished samples. Cleaning processes involving chemical etching result in a surface, which is free from a work-hardened layer. Taking that into account and combining it with the observed nucleation mechanism which differs from that on the mechanically finished surfaces, it is believed that the metal microstructure combined with other features of the surface i.e. inclusions, vacant inclusion locations play a dominant role on hydride initiation and growth.

We believe that, it is the interplay of the microstructural characteristics of the surface and the level of strain present that controls the early corrosion behaviour of uranium by D_2. The key point that this study has revealed is that strain, in addition to microstructure, exerts a significant influence on hydride nucleation and early stage growth morphology. More pragmatically, we have shown that uranium surfaces prepared in different ways will exhibit different hydride formation behaviour. It is likely this will also occur for other metal-hydride systems and indicates that surface finish and strain should be considered when designing corrosion experiments to mimic real-world corrosion scenarios applicable to uranium or uranium metal waste in storage.

Conclusions

The work presented here shows a distinct difference in uranium hydride growth rates and characteristics between different uranium surface preparation methods. It has been observed that the initial lateral and vertical growth rates of the arising hydrides were most affected by the different preparations, thus the level of surface strain, with microstructural features present on the surface of the metal acting as a secondary influence, e.g. carbide particles. The primary difference between the two categories of sample preparation is the level of strain present in the surface of the metal leading to distortions in the lattice and abundant slip twinning. The strain in these samples decreases from coarsely finished sample > finely polished sample > nitric acid etched sample > electropolished sample. The greater the surface-strain in the sample, the higher the nucleation density number, indicating a preferred attack of strained versus unstrained metal. However, as the strain is reduced in the chemically etched samples, surface features such as carbides and grain boundaries were observed to become of much greater importance in controlling nucleation location.

Acknowledgements

References

[1] M.M. Baker, L. Less, S. Orman, Uranium + water reaction. Part 1. -Kinetics, products and mechanism, Transactions of the Faraday Society 62 (1966) 2513-2524.

[2] F. Le Guyadec, X. Génin, J. Bayle, O. Dugne, A. Duhart-Barone, C. Ablitzer, Pyrophoric behaviour of uranium hydride and uranium powders, Journal of Nuclear Materials 396 (2010) 294-302.

[3] S. Bazley, J. Petherbridge, J. Glascott, The influence of hydrogen pressure and reaction temperature on the initiation of uranium hydride sites, Solid State Ionics, 211 (2012) 1-4.

[4] R. Arkush, A. Venkert, M. Aizenshtein, S. Zalkind, D. Moreno, M. Brill, M. Mintz, N. Shamir, Site related nucleation and growth of hydrides on uranium surfaces, Journal of Alloys and Compounds 244 (1996) 197-205.

[5] R. Alire, B. Mueller, C.L. Peterson, J.R. Mosley, Reaction kinetics of uranium and deuterium, The Journal of Chemical Physics 52 (1970) 37-46.

[6] J. Condon, E. Larson, Kinetics of the uranium-hydrogen system, The Journal of Chemical Physics 59 (1973) 855-865.

[7] J. Condon, Alternative model for nonstoichiometry in uranium hydride, The Journal of Physical Chemistry 79 (1975) 42-48.

[8] J. Condon, Calculated vs. experimental hydrogen reactions rates with uranium, The Journal of Physical Chemistry 79 (1975) 392-397.

[9] J. Stakebake, Kinetics for the reaction of hydrogen with uranium powder, Journal of The Electrochemical Society 126 (1979) 1596-1601.

[10] J. Bloch, M. Mintz, Kinetics and mechanism of the UH reaction, Journal of the Less Common Metals 81 (1981) 301-320.

[11] J. Kirkpatrick, J. Condon, The linear solution for hydriding of uranium, Journal of the Less Common Metals 172 (1991) 124-135.

[12] G. Powell, W. Harper, J. Kirkpatrick, The kinetics of the hydriding of uranium metal, Journal of the Less Common Metals 172 (1991) 116-123.

[13] G. Powell, R. Ceo, W. Harper, J. Kirkpatrick, The kinetics of the hydriding of uranium metal II*, Zeitschrift für Physikalische Chemie 181 (1993) 275-282.

[14] S. Bazley, T. Nunney, C. Mormiche, B. Hayden, The dynamics of hydrogen adsorption on polycrystalline uranium, Applied Surface Science 254 (2008) 6376-6379.

[15] J. Bloch, F. Simca, M. Kroup, A. Stern, D. Shmariahu, M. Mintz, Z. Hadari, The initial kinetics of uranium hydride formation studied by a hot-stage microscope technique, Journal of the Less Common Metals 103 (1984) 163-171.

[16] J. Bloch, D. Brami, A. Kremner, M. Mintz, Effects of gas phase impurities on the topochemical-kinetic behaviour of uranium hydride development, Journal of the Less Common Metals 139 (1988) 371-383.

[17] J. Bloch, M.H. Mintz, The effect of thermal annealing on the hydriding kinetics of uranium, Journal of the Less Common Metals 166 (1990) 241-251.

[18] D. Moreno, R. Arkush, S. Zalkind, N. Shamir, Physical discontinuities in the surface microstructure of uranium alloys as preferred sites for hydrogen attack, Journal of Nuclear Materials 230 (1996) 181-186.

[19] D.F. Teter, R.J. Hanrahan, C.J. Wetteland, Uranium hydride nucleation kinetics: effects of oxide thickness and vacuum outgassing, Los Alamos National Lab., NM (US) 2001.

[20] T.B. Scott, G.C. Allen, I. Findlay, J. Glascott, UD_3 formation on uranium: evidence for grain boundary precipitation, Philosophical Magazine 87 (2007) 177-187.

[21] J. Knowles, I. Findlay, D. Geeson, S. Bazley, The influence of vacuum annealing on the nucleation and growth kinetics of uranium hydride, MRS Proceedings, Cambridge Univ Press, 2012, pp. mrss12-1444-y1410-1410.

[22] N. Harker, T. Scott, C. Jones, J. Petherbridge, J. Glascott, Altering the hydriding behaviour of uranium metal by induced oxide penetration around carbo-nitride inclusions, Solid State Ionics 241 (2013) 46-52.

[23] J.P. Knowles, I.M. Findlay, The influence of vacuum annealing on the uranium–hydrogen reaction, Journal of Alloys and Compounds 645 (2015) S230-S233.

[24] C.P. Jones, T.B. Scott, J.R. Petherbridge, J. Glascott, A surface science study of the initial stages of hydrogen corrosion on uranium metal and the role played by grain microstructure, Solid State Ionics 231 (2013) 81-86.

[25] J. Glascott, A model for the initiation of reaction sites during the uranium–hydrogen reaction assuming enhanced hydrogen transport through thin areas of surface oxide, Philosophical Magazine 94 (2014) 221-241.

[26] B. Frost, The carbides of uranium, Journal of Nuclear Materials 10 (1963) 265-300.

[27] J. Bingert, R. Hanrahan, R. Field, P. Dickerson, Microtextural investigation of hydrided α-uranium, Journal of Alloys and Compounds 365 (2004) 138-148.

[28] M. Hill, R. Schulze, J. Bingert, R. Field, R. McCabe, P. Papin, Filiform-mode hydride corrosion of uranium surfaces, Journal of Nuclear Materials 442 (2013) 106-115.

[29] A. Banos, T.B. Scott, Statistical analysis of UH3 initiation using electron back-scattered diffraction (EBSD), Under publication with Solid State Ionics.

[30] L. Owen, R. Scudamore, A microscope study of the initiation of the hydrogen-uranium reaction, Corrosion Science 6 (1966) 461-468.

[31] P. Shi, L. Shen, B. Bai, D. Lang, L. Lu, G. Li, X. Lai, P. Zhang, X. Wang, Preferred hydride growth orientation of U− 0.79 wt.% Ti alloy with β + U_2Ti microstructure, Journal of Nuclear Materials 441 (2013) 1-5.

[32] C. Stitt, C. Paraskevoulakos, N. Harker, C. Jones, T. Scott, The effects of metal surface geometry on the formation of uranium hydride, Corrosion Science 98 (2015) 63-71.

[33] A. DeMint, J. Leckey, Effect of silicon impurities and heat treatment on uranium hydriding rates, Journal of Nuclear Materials 281 (2000) 208-212.

[34] C.P. Jones, T.B. Scott, J.R. Petherbridge, Structural deformation of metallic uranium surrounding hydride growth sites, Corrosion Science 96 (2015) 144-151.
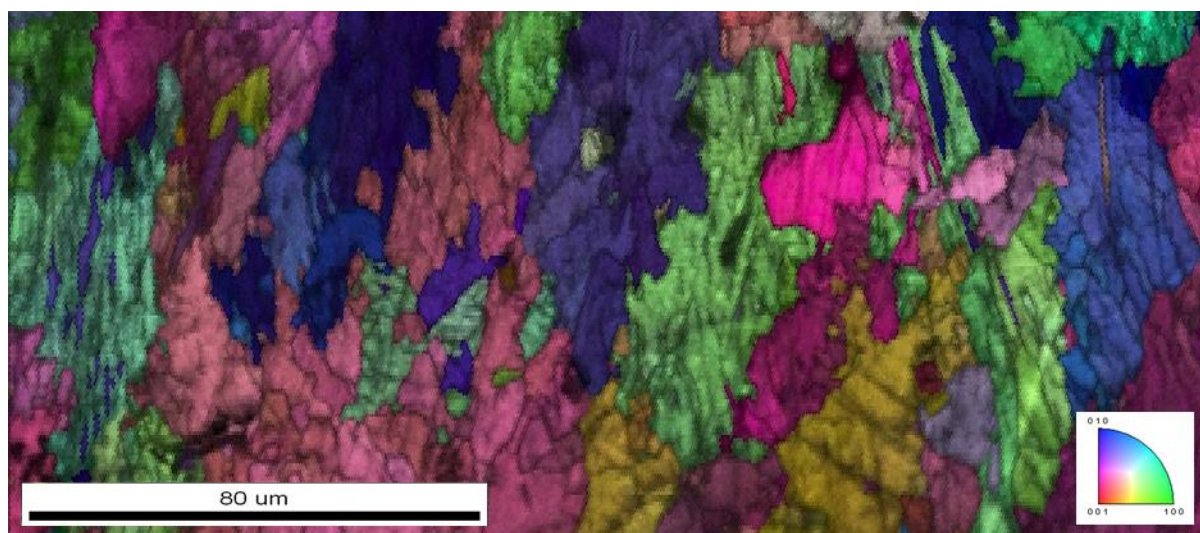
Figure 1: Inverse pole figure - Electron back-scattered diffraction map of the as-received Magnox-U surface.
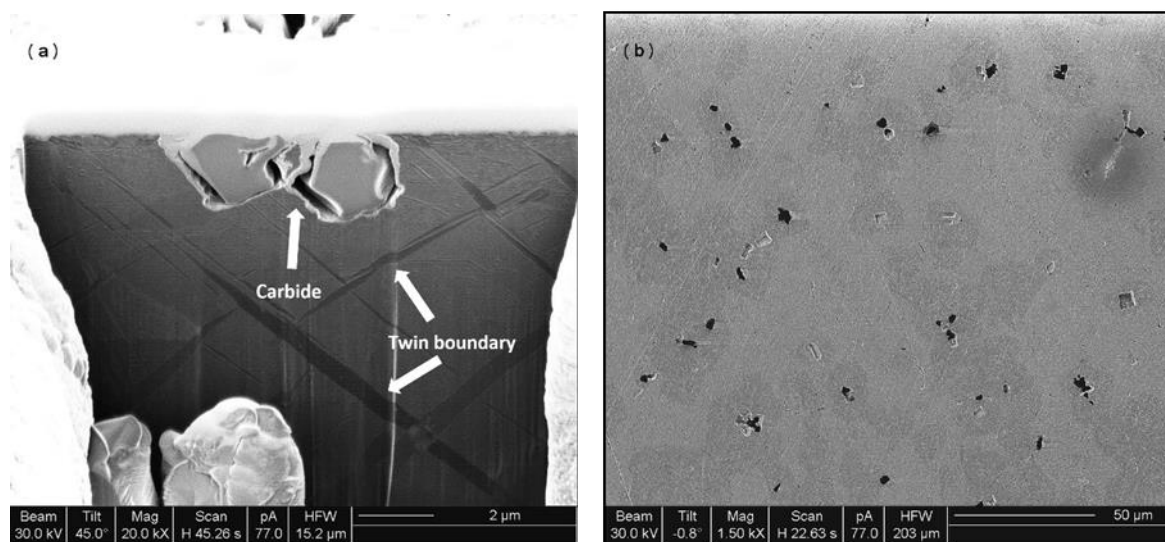

Figure 2: Secondary electron image aqcuired from a focused ion beam (FIB) instrument showing (a) the cross-sectional face of Magnox-U around an inclusion site and (b) the surface of the same sample. The sample was etched in nitric acid to reveal the microstructural features. The FIB imaging revealed a highly strained bulk with conjugate set of intersecting crystal twins (a).
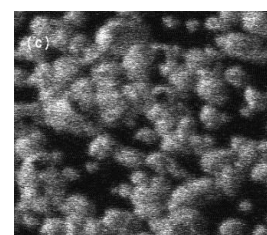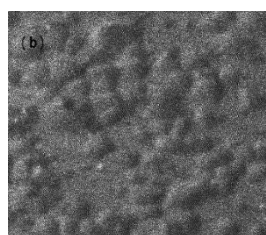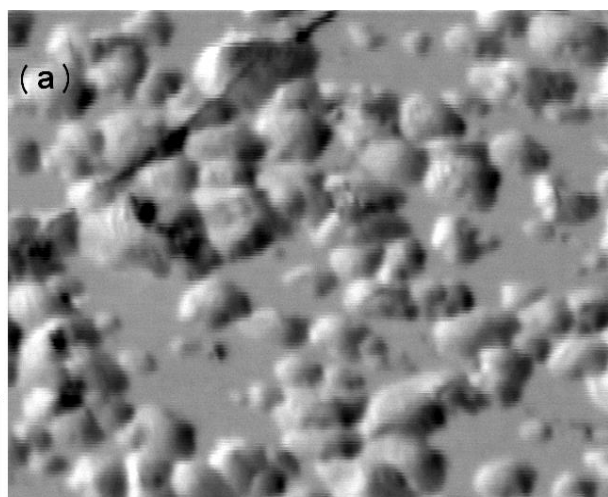
12

Figure 3: Secondary ion mass spectrometry generated SE image of (a) the finely polished sample following hydriding. Intensity map of the surface for the corresponding (b) U$^+$ ion map (mass 238) (c) UH$^+$ ion cluster map (mass 240) (c) UD$^+$ map (mass 242) and (d) UO$_2^+$ map (mass 270).
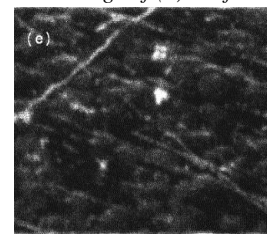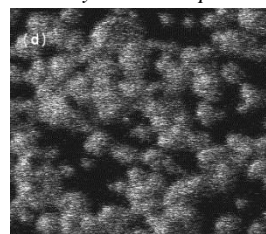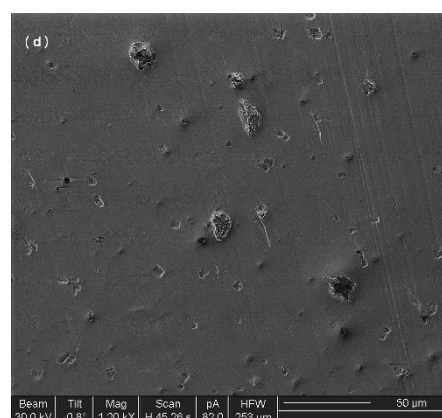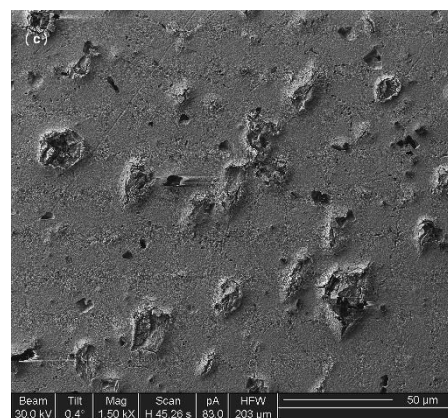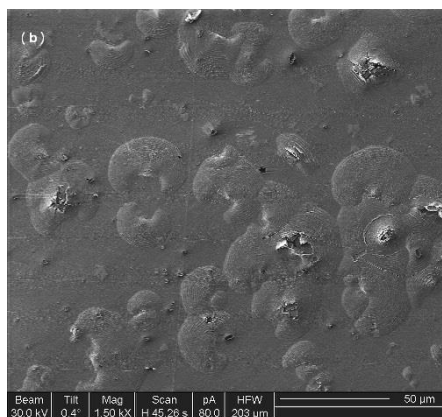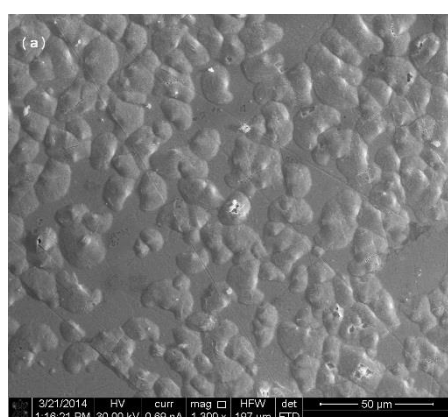

Figure 4: Secondary electron images of (a) the coarsely finished sample (b) the finely polished sample (c) the nitric acid etched sample and (d) the electropolished sample after simultaneous partial hydrogenation.
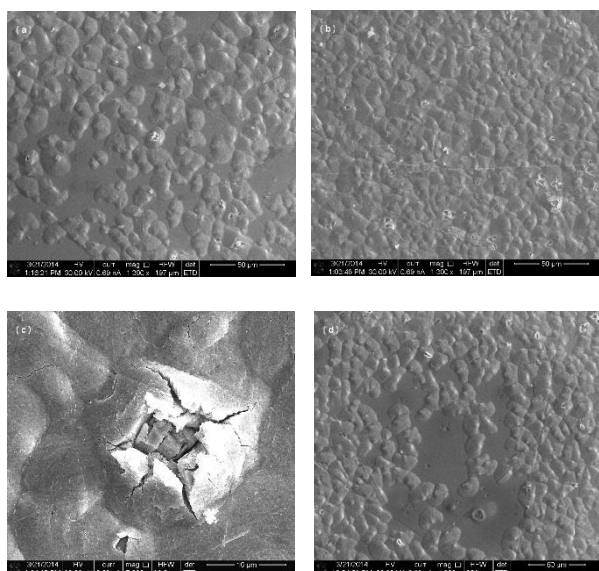
13

Figure 5: Secondary electron images showing (a) the surface topography of the coarsely finished sample following hydrogen exposure; (b) a region of the sample where an almost fully formed surface UH$_3$ layer has developed; (c) An 'oxide burst' hydride forming around a carbide inclusion particle and (d) a less-attacked region of the surface.
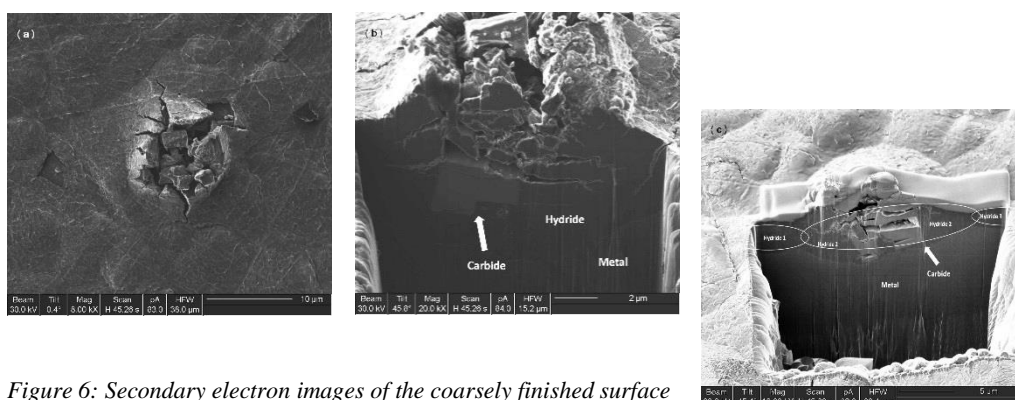

Figure 6: Secondary electron images of the coarsely finished surface depicting (a) a hydride growth site breaching the oxide surface and (b)-(c) FIB cross-sectional cuts of two separate hydrides confirming the presence of a carbide at the centre, which has been split by hydride formation. On (c) circled areas highlight the propagation of hydride peripheries for three neighbouring hydrides. High nucleation rate and density combined with high lateral growth leads to coalescence of the neighbouring hydrides and hence further lateral growth suppression.
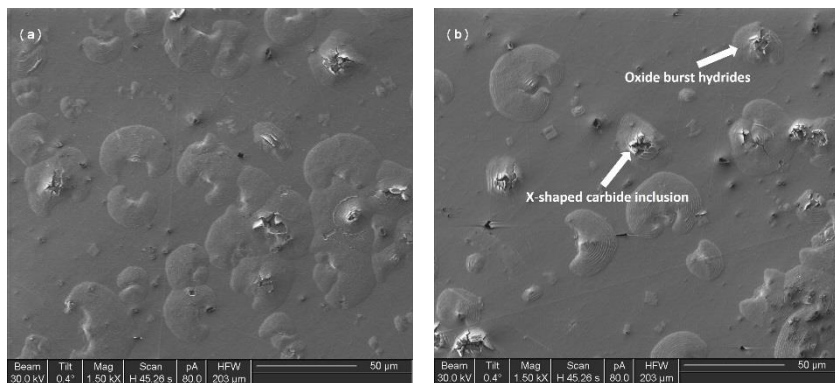
14

Figure 7: Secondary electron images showing (a) the hydrided surface of the finely polished sample and (b) hydride burst sites coinciding with carbide inclusions.
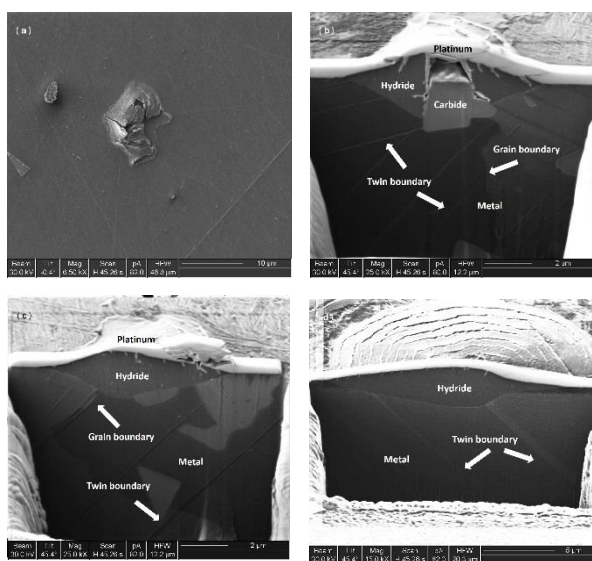

Figure 8: Secondary electron images of the finely polished surface illustrating (a) a hydride forming around an inclusion; (b) a cross-sectional cut of the same site confirming the existence of a grain boundary along with multiple twin boundaries crossing the growth centre of the spot. On (c) and (d) two focused ion beam cross-sectional cuts of various non oxide-breached hydrides forming at a grain and twin boundary site, respectively.
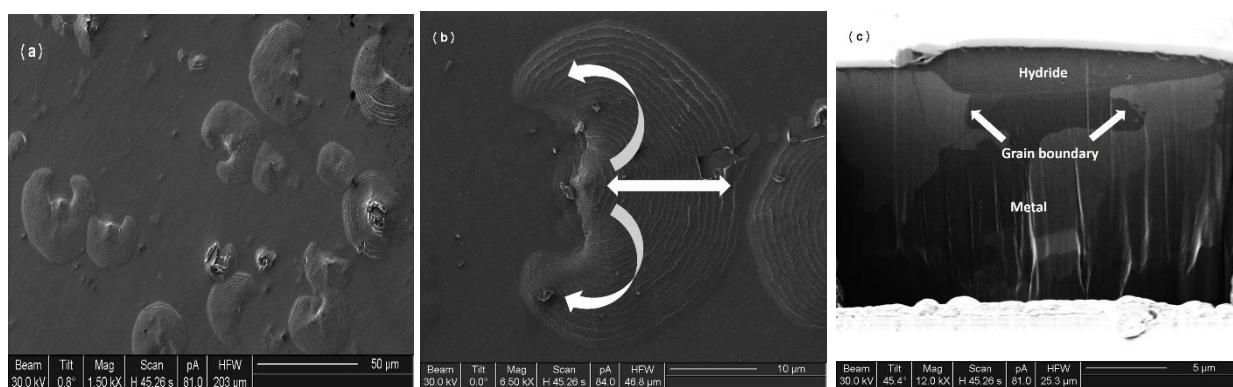
Figure 9: Secondary electron images depicting (a) multiple crescent shaped UH₃ formation on the surface of the finely polished sample; (b) the growth mechanism of a hydride of this type (the arrows highlight the growth direction) and (c) a cross-sectional face of the same hydride revealing the preference of these sites to nucleate on grain boundaries.
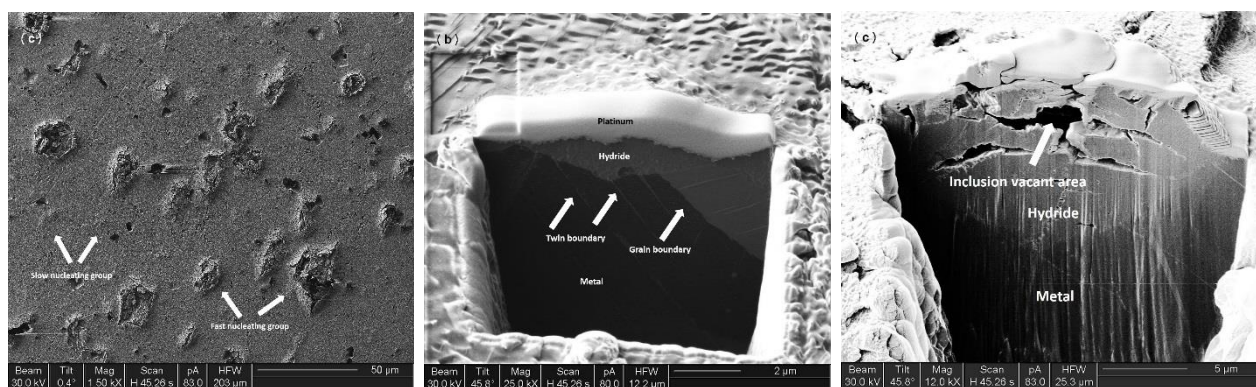

Figure 10: Secondary electron images showing (a) the reacted surface of the nitric acid etched sample revealing two UH₃ families; (b) a hydride of the small nucleating group forming on a grain boundary and (c) a burst UH₃ site forming on a location where a carbide particle was ascribed to have pre-existed.

16

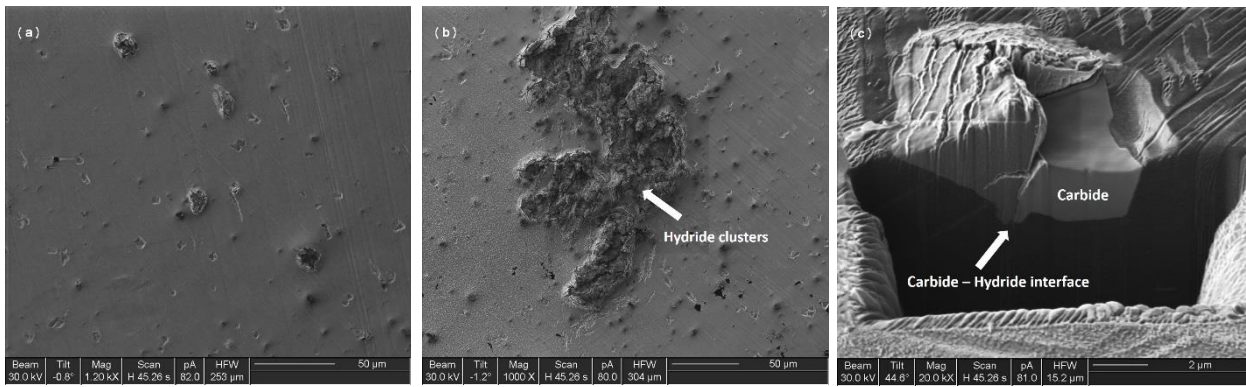*Figure 11: Secondary electron images showing (a) the post-hydrided surface of the*

electropolished sample; (b) a cluster of large diameter and burst hydrides and (c) a hydride nucleating at the margins of an inclusion site.
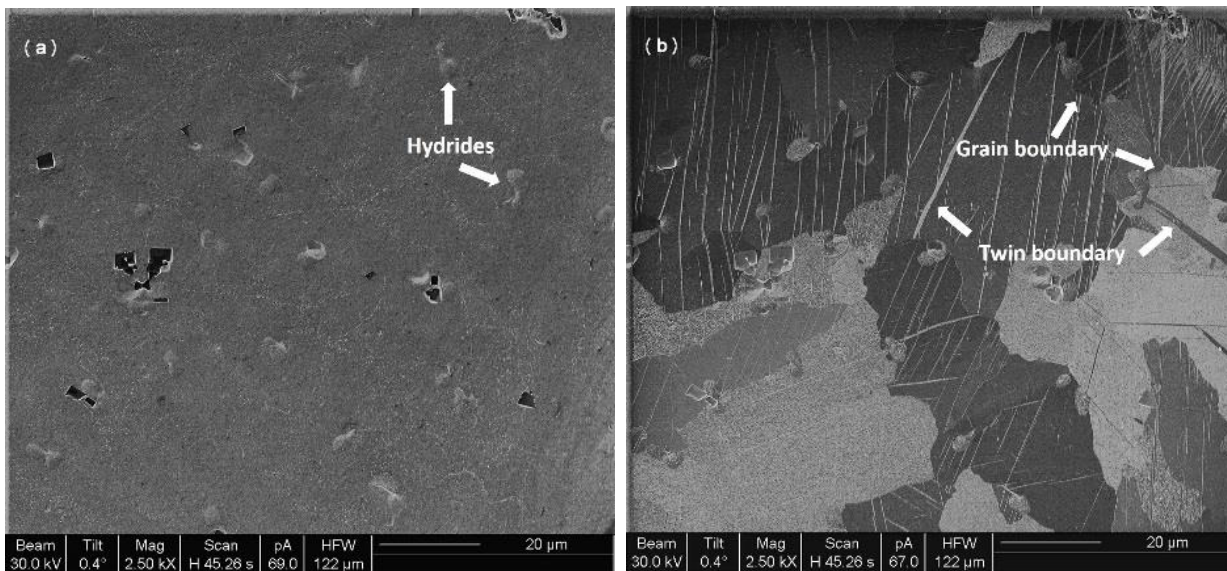
Figure 12: Secondary electron images of the

electropolished and partially hydrided surface a) before ion-sputtering and b) after ion-sputtering for 5 minutes (6600 pA).

17
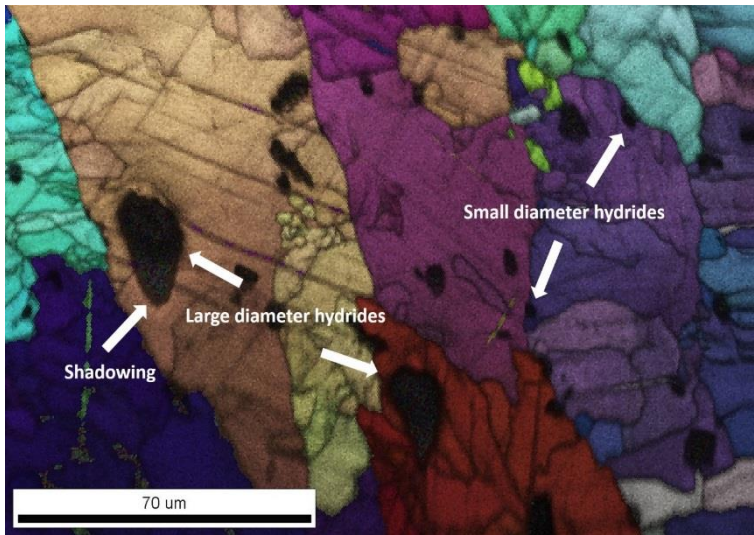
Figure 13: Electron back-scattered diffraction map of the electropolished and spot-hydrided surface. Large diameter and small diameter hydride spots are forming mainly around grain and twin boundaries.

Figure 14: A secondary electron image of a cross-sectional cut of a hydride on the finely polished surface. The red arrows highlight the numerator and denominator of the aspect ratio.

18

Table 1: Summary of uranium hydriding conditions and corrosion behaviour at the early stage.

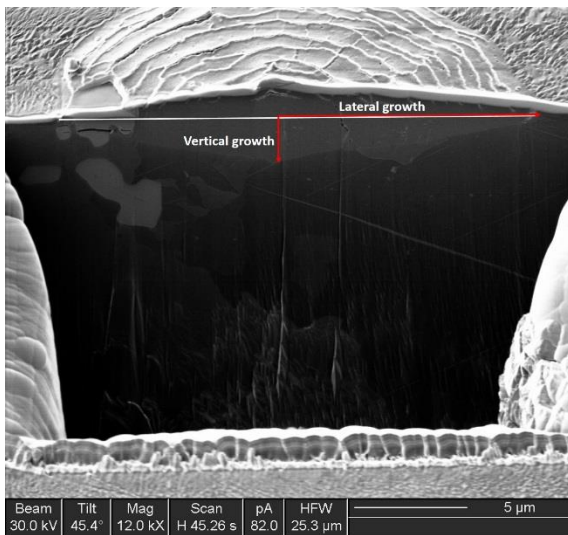| Sample	Impurities (ppm)	Thermal treatment	Shape	Cleaning preparation	T (°C)	Gas pressure (mbar)	Oxide thickness (nm)	Hydride family type	Location	Nucleation rate	Growth rate (parallel/vertical)	Reference
U	> 500	Vacuum cast and extruded	Cylinder (6.35 x 3.175 mm)	Mechanically polished and electropolished	170	933.25	<5 (Air-grown oxide)	1st family: Small diameter spots evenly distributed. 2nd family: Large nodular spots breaching the oxide and formed in clusters	2nd family: Inclusions	1st family: High. 2nd family Low	1st family: Low/ Low. 2nd family: High/High	[30]
U	C ~90, Fe ~22, Cu ~45, Ti< 10	n/a	Cylinder	Mechanically polished	<150	1333	n/a	Hydride nuclei (3-10 µm)	Slip planes, Grain boundaries	n/a	n/a	[15]
U	n/a	Thermally annealed	Disc (2 x 0.6 mm)	Cleaned in 50% HNO₃	100-200	500	<20 (Estimated value)	Large pitted hydrides	n/a	Low	High	[17]
U	C ~90, Fe ~22, Cu ~45, Ti< 1	n/a	n/a	Mechanically polished up to 1µm following 200 °C for 2 h in vacuum	50-75	1000	~4	1st family: Small (sub-micron sized) fast nucleating spots. 2nd family: Larger blister-like hydrides	1st family: Polishing scratches. 2nd family: Inclusions	1st family: High. 2nd family Low	1st family: Low/ Low. 2nd family: High (5µm/min)/ High	[4]
U-0.1Cr	C ~550, Fe ~45, Si ~90, Cu <10	n/a	n./a	Mechanically polished up to 1 µm, electrolytically etched and kept in vacuum (200 °C, 2 h	50-75	1000	50	1st family: Small diameter fast nucleating spots. 2nd family: Larger blister-like hydrides. 3rd family: Very large hydride nuclei	1st family: No specific preference. 2nd family: Perimeter of inclusions (inclusion swelling). 3rd family Not inclusion centred	1st family: High. 2nd family: Low. 3rd family: Low	1st family: High (6 µm/min)/ High. 2nd family Low/Low. 3rd family Moderate (0.8 µm/min)/ Moderate	[4]
U	C:30, Al:7, Cu:9, Fe<10, Mn:15, Ni:14, Si:28, Ti:6, Cr<2	Swanging from 20 to 3.18 mm, thermally annealed α-β phase	Rod	Nitric acid etched	200	10666	n/a	n/a	n/a	n/a	n/a	[33]*
U	<300	Thermally annealed	Rod	Electropolished, baked at 100 °C and exposed to air	70	1013	250	Large pitted hydrides	n/a	n/a	n/a	[19]
U	C: 100-300	Cast	Cylinder (5 x 10 mm)	Mechanically polished and electropolished in H₃PO₄	70	800-870	n/a	1st family: Small non-breached hydrides. 2nd family: Larger pitted hydrides	1st family: Intragranularly. 2nd family: Low and high angle grain and twin boundaries	1st family: High. 2nd family: Low	1st family: High/ High. 2nd family: Low/ Low	[27]
Depleted-U	C <50	n/a	Square coupon (10 x 1 mm)	Mechanically polished down to 3 µm in inert atmosphere, thermally annealed at 550 °C for 16 h, 5 min in air and annealed at 75 °C for 12 h.	320	500 (D₂)	<20	Quasi-spherical growth chains (<1 µm)	High angle grain and twin boundaries	High	Low/Low	[20]
Depleted-U	C: 600	Cast	Disc (15 x 1 mm)	Mechanically polished 2-3 µm and left in air for 5 min	240	525	<10	Hydride nuclei of various sizes	Around margins of Inclusions	High	Low/Low	[22]
Depleted-U	C: 600	Cast	Disc (15 x 1 mm)	Mechanically polished 2-3 µm and electropolished	240	525	<10	Large diameter pitted hydrides (30-600µm)	Not associated with inclusions- Not specified	Low	High/High	[22]
Depleted-U	Si:1090, C:625, Fe:115, Mo:57, Ni:85, Al:70, Cr:46, Cu:24, Zr:11	Cast and arc-melted	Rod (11 x 2 mm)	Mechanically polished up to 1 µm in an inert atmosphere, electropolished, Ar⁺ sputtered and left in vacuum at 70 °C for 6 days.	25	267 He- 67 H₂	<7	Filiform-like extensions	Grain and twin boundaries	Filiform-like corrosion	Filiform-like corrosion	[28]
Depleted-U	Si:1090, C:625, Fe:115, Mo:57, Ni:85, Al:70, Cr:46, Cu:24, Zr:12	Cast and arc-melted	Rod (11 x 2 mm)	Mechanically polished (600 grit) in an inert atmosphere	n/a	267 He- 67 H₂	>10	Small circular hydride nuclei evenly distributed	Discontinuous work-hardened layer	High	Low/Low	[28]
Depleted-U	Si:1090, C:625, Fe:115, Mo:57, Ni:85, Al:70, Cr:46, Cu:24, Zr:13	Cast and arc-melted	Rod (11 x 2 mm)	Mechanically polished (600 grit) in air	n/a	267 He- 67 H₂	>>10	Large circular hydride nuclei	Discontinuous work-hardened layer	Low	High/High	[28]
Depleted-U	C <50	n/a	Square coupon (10 x 1 mm)	Mechanically polished up to 1 µm in an inert atmosphere	240	500	n/a	Non breached spots ~2 µm	Grain boundaries	High	Low/Low	[24]
Depleted-U	C <50	n/a	Square coupon (10 x 1 mm)	Work-hardened layered surface: Mechanically polished 46 µm-10 µm-1 µm	240	500	n/a	Large pitted hydrides	Carbide inclusions	Low	High/High	[24]

*Included to highlight the nitric acid etched preparation.

19

Table 2: Average oxide thickness of all four samples using secondary ion mass spectrometry depth profiling.

Sample	Average thickness after 1 hour in air (nm)
Coarsely finished	40.0
Finely polished	34.3
Nitric acid etched	44.6
Electropolished	19.8

Table 3: The parameters of the hydride sites.

Sample	Spatial nucleation density (hydrides/mm²)			Small diameter family - Non burst sites (µm)			Large diameter family (µm)		
	Min	Max	Average	Min	Max	Average	Min	Max	Average
Coarsely finished	1875	6875	4761.74	n/a	n/a	n/a	13	30	21.65
Finely polished	175	925	536.1	n/a	n/a	n/a	9	42	26.98
Nitric acid etched	25	625	261.9	7	15	11.24	15	40	25.8
Electropolished	0	325	88.27	10	25	18.19	33	70	44.24

Table 4: Ratio of lateral to vertical hydride growth.

Sample	Hydride depth (µm)			Ratio of lateral to vertical growth velocity		
	Min	Max	Average	Min	Max	Average
Coarsely finished	2.5	5.5	3.77	1.83	5.2	2.9
Finely polished	0.7	4.5	2.03	3.56	12.67	6.31
Nitric acid etched- (Small diameter family)	0.89	2.5	1.55	2.4	5.51	3.93
Nitric acid etched- (Large diameter family)	2.56	9.5	6.09	1.77	4.4	2.45
Electropolished- (Small diameter family)	0.93	3.62	2.47	2.76	4.08	3.45
Electropolished- (Large diameter family)	n/a	n/a	n/a	n/a	n/a	n/a